Journal of Electrical and Computer Engineering Innovations
(JECEI)
Journal homepage: http://www.jecei.sru.ac.ir

Research paper

Torque Ripple Reduction and Fault-Tolerant Control of Non-Sinusoidal DTP-PMBLM Fed by Two DC3L Inverters Using Model Predictive Control

Zahra Emami , ***Abolfazl Halvaei Niasar*** *

Department of Electrical & Computer Engineering, University of Kashan, Kashan, Iran.

Article Info

Article History:
Received 05 June 2025
Reviewed 28 July 2025
Revised 20 September 2025
Accepted 27 September 2025

Keywords:
Non sinusoidal DTP-PMBLM
Model Predictive Control (MPC)
Diode-Clamped Three-Level (DC3L) inverter
Multiband Hysteresis Current (MHC) controller
fault-Tolerant Control (FTC)

*Corresponding Author's Email Address:
halvaei@kashanu.ac.ir

Abstract

Background and Objectives: Multiphase electric motors are useful for industrial and military applications that need high power, smooth torque and the ability sharing power and torque in comparison to conventional three-phase electric motors. Also, these motors a more suitable substitute than three-phase motors because of their ability to manage fault condition, guaranteeing the postfault operation of the drive. One type of Multiphase electric machines is Permanent Magnet Brushless Motors (PMBLM) that due to the inevitable limitations in their construction, back-EMF voltages are neither sinusoidal nor trapezoidal. Using traditional control strategies of and Brushless DC Motors (BLDCM) and Permanent Magnet Synchronous Motors (PMSM) results high electromagnetic torque ripple, vibrations and noises that are undesirable for medium voltage applications.
Methods: This paper suggests a new finite control set model predictive control (FCS-MPC) method for two diode-clamped three-level (DC3L) inverters fed by non-sinusoidal dual three-phase PMBLM (DTP-PMBLM), with the capability to manage pre-fault conditions for torque ripple reduction and withstand post-fault situations. The suggested MPC method removes the requirement of a weighting factor in the cost function for neutral-point voltages in both DC3L inverters, with a simple capacitive voltage balancing scheme. Also, the fault-tolerant control (FTC) schemes for open-phase faults and open-switch faults are considered.
Results: To study the effectiveness of the suggested MPC method, simulation results non-sinusoidal DTP-PMBLM drive are investigated and compared to with multiband hysteresis current (MHC) controller. Simulations have been carried out using MATLAB/Simulink with specifications 4125-V/2.7MW/350-RPM.
Conclusion: Simulation results validate that the proposed MPC method provides superior dynamic performance, including lower torque ripple compared to the MHC controller. The FTC schemes are implemented without increasing complexity or changing the mathematical model and control framework.

This work is distributed under the CC BY license (http://creativecommons.org/licenses/by/4.0/)

How to cite this paper:
Z. Emami, A. Halvaei Niasar, "Torque ripple reduction and fault-tolerant control of non-sinusoidal DTP-PMBLM fed by two DC3L inverters using model predictive control," J. Electr. Comput. Eng. Innovations, 14(1): 265-284, 2026.
DOI: 10.22061/jecei.2025.11739.841
URL: https://jecei.sru.ac.ir/article_2431.html

2345- 3044/© 2026 The Authors. Published by Shahid Rajaee Teacher Training University.

Introduction

Multiphase electric motors are beneficial for industrial and military applications that need high power, smooth torque and low torque pulsation, fault tolerance, lower current stress for switching devices, and more degrees of control freedom compared to traditional three-phase electric motors [1]-[3]. A type of multi-phase motors that is very widely used is asymmetric six-phase PMSM motors, which have the ability to further reduce the torque ripple of the motor and increase the reliability of the drive. In these motors, which are called DTP-PMSM for short, the stator has two categories of three-phase windings with separate star connections, and the same windings in each group have a spatial phase difference of 30 degrees compared to each other [4]-[6]. Due to the high number of phases and the high current of the motor windings and Limitation in design and construction, it is not possible to distribute the sinusoidal flux of DTP-PMSM motors and as a result, the back-EMF voltages of the motor are often not pure sinusoid and have higher harmonics. Therefore, the motor under study is a non-sinusoidal (DTP-PMBLM) that containing the first, third, fifth and seventh harmonics. In some special applications such as military, the motor torque ripple causes mechanical vibration or acoustic noise which is not acceptable for military standards.

Available control strategies of multiphase drives in healthy state are FOC [7], DTC [8], [9] Hysteresis control [10]. However, noises, losses and variable switching frequencies are disadvantage of the control methods.

Lately, different model predictive control (MPC) techniques have been suggested and investigated for multiphase motor drives [11], [12].

By combining the non-sinusoidal DTP-PMBLM and the two DC3L inverters, the torque ripple will be less and the performance of the drive system will be improved. In the medium voltage (MV) drives of AC motors that are fed by PWM inverters, the voltage and current values are high. Hence, diode-clamped three-level (DC3L) inverter is a suitable alternative compared with two-level inverters. Reduction of voltage stress on inverter switches and reduction of voltage harmonics applied to the motor and reduction of switching losses and less electromagnetic interference are advantages of these inverters [13]-[15]. Furthermore, other challenge is unbalancing of neutral point (NP) voltage in the DC3L inverters that cause harmonics in the load and high voltage stress in switching devices. In [16], balancing the voltage of the capacitors in the DC3L inverter uses an extra weighting factor which is tedious to adjust.

The fault-tolerant control (FTC) ability is the most attractive issue in multiphase drives. This field has been widely researched for three phase motors under faulty conditions [17] and the FTC schemes for current, speed, and torque control [18], [19] has been expressed.

However, FTC capability can only be obtained with additional electrical instruments [20], which increases weight and the cost and of the inverter and the complication of the three-phase motor drive.

The status is different in multiphase motors where no additional equipment is needed to obtain FTC. Multiphase drive systems have more degrees of freedom due to the high number of phases [21].

FTC for multiphase drives is performed in several ways. 1) the creation of new current references for FTC with constraints on voltage, current and copper loss optimization. Once one or more phases are open in the circuit, new current references are defined by reconfiguration, which is called reconfiguration [22], [23] 2) modeling of multiphase drives for FTC [24]. 3) Based on kinds of magnetomotive force (MMF)s for FTC. FTC strategies for sinusoidal multiphase motors have been presented in [7], [25], [26] FTC schemes for sinusoidal motors are easily used to non-sinusoidal motors due to torque ripples. In [22], [27], [28] have been presented FTC schemes for non-sinusoidal multiphase electrical motors. These schemes are more complex than sinusoidal motor strategies. 3) Based on modeling of multiphase electrical motors for FTC performances including Clarke transformation of healthy mode [7], reduced-order transformation matrices [29]. 4) Based on control techniques for FTC operations the classical FOC scheme [7], MPC [11], DTC [29] , Hysteresis control [30], and Robust control [31]. In [32] for MPC strategy for Dual Three-Phase PMSM with two DC3L inverters has been has been implemented. But the voltage and power levels are low and the switching frequency is low. Also, motor is Pure sinusoidal and non-harmonic. Therefore, naturally the torque and current ripple are less than suggested MPC strategy.

By reviewing previous researches that have been done in multiphase electric motors control was observed that each of the methods, despite their many uses, however, they still face challenges such as high torque ripple pre-fault and complex processes of reconstruction the machine model and control scheme are the basic challenging of previous fault-tolerant control schemes of multiphase drives.

Hence, this paper proposes the suggested MPC strategy that focuses on reducing the torque ripple to eliminate mechanical vibration or acoustic noise that is unacceptable in sensitive medium voltage applications. Since tuning the weight factors is challenging, a method to balance the capacitor voltage without the need for a weighting factor is presented to eliminate a capacitor balancing objective in the cost function, which leads to the reduction of torque ripple. Also, other aim using the suggested MPC strategy is used to manage the control of

the non-sinusoidal (DTP-PMBLM) drive both in pre-fault and postfault conditions.

The results of the suggested MPC method are compared and analyzed with the multiband hysteresis current (MHC) controller method through simulation. Hence, the paper contains the following sections: the model of non-sinusoidal DTP-PMBLM and the performance of DC3L inverter, the suggested MPC strategy and comparing with the MHC controller, the presented method for DC3L inverter capacitor voltage balancing, the proposed FTC schemes and finally the conclusion.

Simulations have been accomplished in MATLAB/Simulink that evaluate the conceivability and implementation of the suggested MPC strategy with specifications of 4125-V/2.7-MW/350-RPM non-sinusoidal DTP-PMBLM. The suggested MPC approach presents lower torque ripple and better quantitative and qualitative features in comparison with the MHC control approach. The FTC schemes are presented for two kinds of prevalent electric faults in the two DC3l inverters fed non-sinusoidal DTP-PMBLM with fixing the mathematical model and control strategy. Hence, the FTC schemes can be implemented simply and smooth dynamic response can be ensured.

System Configuration and Modeling

MTP PMSM modeling methods are divided into two groups: vector space decomposition model [33] and individual multiple three-phase model [34]. In using the VSD model analytical and mathematical modeling of MTP PMSM is done in orthogonal subspaces. In this method, the motor model is formulated by using one αβ subspace and different xy subspaces and zero sequence components. The VSD transformation is able to separate the harmonics and put them in each subspace. In this paper, the under study motor is investigated in the dual individual αβ reference frame. Table 1 shows the notation for parameters and variables used in this paper.

Fig. 1(a) shows the configuration of the DC3L six-phase inverters fed non-sinusoidal DTP-PMBLM including two sets of three-phase star windings which is shifted by 30 electrical degrees and the neutral points of the two sets of three-phase star windings are isolated.

Fig. 1(b) shows the configuration of non-sinusoidal DTP-PMBLM. The mutual inductance are described by (1) [35]:

$$M_{ij} = \frac{2}{3} L_m \cos(\theta_i - \theta_j) = \frac{2}{3} L_m \cos(\Delta\theta_{ij}) \quad (1)$$

The rotor electrical positions of stator windings are shown by θ_{ei}, θ_{ej} and L_m is magnetizing inductance. The electrical displacements one of the three-phase windings are $0, \pm 120^{\circ}, \pm 240^{\circ}$. Also, the electrical displacements the first and the second three-phase winding are $\pm 30^{\circ}, \pm 150^{\circ}, \pm 270^{\circ}$, separately. The voltage vector can be can be written as below form [35]:

$$\overrightarrow{\boldsymbol{u_s}} = \boldsymbol{R_s}\vec{\boldsymbol{i_s}} + [\boldsymbol{L}]\frac{d\vec{\boldsymbol{i_s}}}{dt} + \vec{\boldsymbol{e}} \quad (2)$$

Table 1: Notation for parameters and variables

symbol	Description
L_m	Main inductance
$\boldsymbol{R_s}$	Stator resistance matrix
$\boldsymbol{L}$	Stator inductance matrix
L_{s1}	Primary stator inductance matrix
L_{s2}	Secondary stator inductance matrix
$\boldsymbol{u_s}$	Primary voltage vector
$\boldsymbol{I_s}$	Stator current vector
$\boldsymbol{M_{s1}}$	Primary mutual inductance matrix
$\boldsymbol{M_{s2}}$	Secondary mutual inductance matrix
L_{ls}	leakage inductance
$\boldsymbol{e}$	Back-EMF vector
$V_C^{\ T}$	DC voltage of capacitor in first inverter
$V_C^{\ B}$	DC voltage of capacitor in second inverter
Vn	neutral point voltage
Te	Electromagnetic torque
$\boldsymbol{L_{\alpha\beta}}$	Inductance matrix in Stationary reference frame
$\boldsymbol{R_{\alpha\beta}}$	Stator resistance matrix in Stationary reference frame
T_s	Sampling time
T_{e1}	electromagnetic torque in first winding set
T_{e2}	Electromagnetic torque in second winding set
ω_m	Rotor mechanical speed
θ_e	Angular position of the rotor
$\boldsymbol{i_{\alpha\beta}}$	Current in Stationary reference frame

$$\boldsymbol{L_{s1}} = \boldsymbol{L_{s2}} = \frac{2}{3}\begin{bmatrix} \frac{3}{2}L_{ls} + L_m & -\frac{1}{2}L_m & -\frac{1}{2}L_m \\ -\frac{1}{2}L_m & \frac{3}{2}L_{ls} + L_m & -\frac{1}{2}L_m \\ -\frac{1}{2}L_m & -\frac{1}{2}L_m & \frac{3}{2}L_{ls} + L_m \end{bmatrix} \quad (3)$$

$$\boldsymbol{M_{s1}} = \frac{2}{3}L_m\frac{\sqrt{3}}{2}\begin{bmatrix} 1 & -1 & 0 \\ 0 & 1 & -1 \\ -1 & 0 & 1 \end{bmatrix} \quad (4)$$

$$\boldsymbol{M_{s2}} = \frac{2}{3}L_m\frac{\sqrt{3}}{2}\begin{bmatrix} 1 & 0 & -1 \\ -1 & 1 & 0 \\ 0 & -1 & 1 \end{bmatrix} \quad (5)$$

$$\boldsymbol{L} = \begin{bmatrix} L_{s1} & M_{s1} \\ M_{s2} & L_{s1} \end{bmatrix} \quad (6)$$

where $\vec{u}_s$, $\vec{i}_s$ and $\vec{e}$ are six-dimensional phase voltages, currents and back-EMF voltages vectors, respectively; R_s is a six by six stator resistance diagonal matrix that describes stator resistance of windings; *L* is six by six stator inductance matrix and M_{s1}, M_{s2} are mutual inductances that is shown in (6). All phases have considered with same leakage inductance L_{ls}.

It is noteworthy that non-sinusoidal DTP-PMBLM with phase back-EMF have been created using sinusoidal functions in created motor of MATLAB/Simulink and are including the harmonics of order 1,3,5 and 7 that their amplitude percentage is 100%, 30%, 10% and 5% respectively. The back-EMF voltage of a1 phase in first 3-phase winding and the back-EMF voltage of a2 phase in second 3-phase winding are expressed as:

$$e_{a1}(t) = E_1 \sin \omega t + E_3 sin3\omega t + E_5 sin5\omega t + E_7 sin7\omega \quad (7)$$

$$e_{a2}(t) = E_1 \sin(\omega t) + E_3 sin3(\omega t - \frac{\pi}{6}) + E_5 sin5(\omega t - \frac{\pi}{6}) + E_7 sin7(\omega t - \frac{\pi}{6}) \quad (8)$$

Modeling of DC3L Inverter

The DC3L inverter configuration is represented in Fig. 1(a). Each set of three phase winding are fed from a separate DC3L inverter. The voltage of the DC link is V_{DC} and DC capacitors are expressed with C_1 and C_2. Each phase includes switches $S_{x1} \sim S_{x4}$ $(x = a,b,c)$ and clamp diodes. Switching modes of the DC3L inverter is shown in Table 2.

Table 2: Switching modes of DC3L inverter

Switching state	P	O	N
S_{x1}	1	0	0
S_{x2}	1	1	0
S_{x3}	0	1	1
S_{x4}	0	0	1
Output Voltage	$V_{DC}/2$	0	$-V_{DC}/2$

There are three switching modes in each phase for three-level inverters. Therefore, there are 27 switching states for the DC3L inverter corresponding to 27 voltage vectors in the space vector diagram, according to Fig. 2. Based on the amplitude, 27 voltage vectors can be can be classified into four types: large vectors are (V15, V17, V19, V21, V23, V25) with magnitude of $(2V_{DC}/3)$, medium vectors are (V16, V18, V20, V22, V24, V26) with magnitude of $(\sqrt{3}/3V_{DC})$, small vectors are (V3~V14) with magnitude of $(V_{DC}/3)$ and zero vectors (V0, V1, V2) [32], [36], [41].

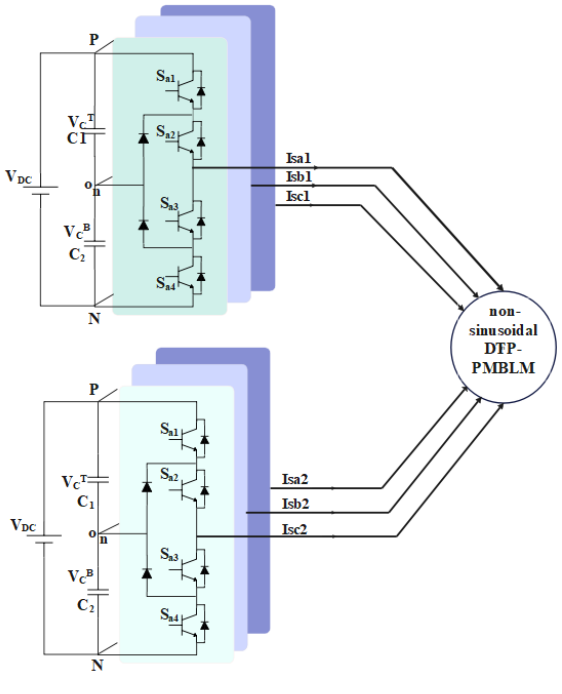

(a)

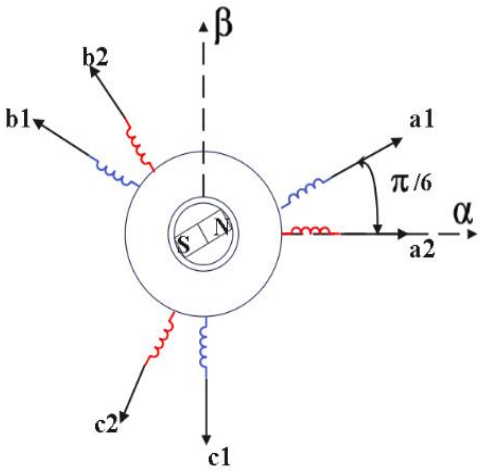

(b)

Fig. 1: (a) drive system (b) non-sinusoidal DTP-PMBLM.

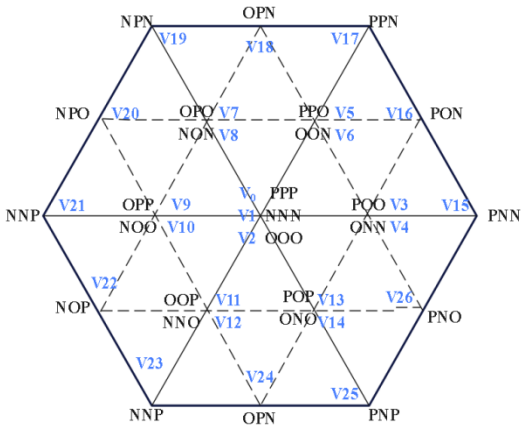

Fig. 2: DC3L Inverter space vector diagram.

The neutral point voltage is written as follows:

$$V_n = \frac{V_C^T - V_C^B}{2} \quad (9)$$

where V_C^T and V_C^B are the DC voltage of capacitors.

The Suggested Control Scheme

For better evaluation, the MHC controller strategy is compared with the suggested MPC method. DTP-BLDCM in the MHC controller similar to the suggested MPC method are fed by two DC3L inverters. Fig. 3(b) illustrates the MHC controller scheme, briefly. The MHC controller for one phase of DC3L inverter needs two symmetrical bands. The actual current from each phase is compared with the reference current which produces an error signal. The error signal is compared by upper hysteresis controller between the up and middle band limit for the upper switches of the inverter leg. Also, the lower hysteresis controller compares the error signal between the low and middle band limit for the lower switches of the inverter leg. The signals produced from hysteresis bands are sent to Hall sensors. Switching pulses are produces based on the output of the hysteresis controllers and Hall sensors inputs. In this method, the rotor speed follows the reference speed through hysteresis bands, which makes each phase follow its reference current. By switching frequency obtains the bandwidth of hysteresis controllers. In simulation, 2% bandwidth is chosen. The reference current I_x^{ref} and the currents I_x are sent to the hysteresis blocks, which includes six hysteresis controllers. These hysteresis blocks specify the proper switching state of phases where x = a1, b1, c1, a2, b2, c2 [37], [38].

As can observed in Fig. 3(b) high electromagnetic torque ripple and current overshoots occur in commutation times, which are significant problems of this strategy.

The MHC controller is strongly dependent the switching frequency. However, the suggested MPC strategy modifies the control loop at medium sampling frequencies. The MHC controller performs better in the 40kHz switching frequency. However, in this simulation, the suggested MPC strategy operates with 20kHz switching frequency well. Hence, the MPC strategy has fewer switching losses than the MHC controller due to the switching frequency reduction. Therefore, the suggested MPC strategy has higher efficiency.

Also, Fig. 3(a) shows the suggested MPC strategy scheme. As are observed the suggested control scheme contains three main parts: (1) the speed control loop that creates reference torque; (2) using of the stationary reference frame for computing of back-EMFs, stator voltage, and stator currents and (3) model predictive control scheme including neutral point voltage balancing, formulation of the cost Function and the FTC schemes.

Stationary reference frame is used for converting back-EMFs, stator voltage and stator currents. For this propose, calculated back-EMF values and measured currents are transferred to the αβ stationary reference frame utilizing the Clark transformation (T) that has been shown in (10). In the space voltage diagram of the DC3L inverter, there are 27 voltage vectors, including 19 impressive voltage vectors and 8 redundant voltage vectors. In this way, using of the MPC method two DC3L inverters needs 19×19=361 various voltage vectors that is calculated by the cost function in each control cycle. The output voltages values of DC3L inverters are calculated by utilizing the DC link voltage and impressive switching states and then is transferred to stationary reference frame. The MATLAB code of the MPC block includes the turquoise blocks shown in Fig. 3(a). The second 3-phase winding is transferred to the αβ reference with a phase shift of 30 electrical degrees.

$$T = \begin{bmatrix} 1 & -\frac{1}{2} & -\frac{1}{2} & 0 & 0 & 0 \\ 0 & \frac{\sqrt{3}}{2} & -\frac{\sqrt{3}}{2} & 0 & 0 & 0 \\ 0 & 0 & 0 & \frac{\sqrt{3}}{2} & -\frac{\sqrt{3}}{2} & 0 \\ 0 & 0 & 0 & \frac{1}{2} & \frac{1}{2} & 0 \\ \frac{1}{3} & \frac{1}{3} & \frac{1}{3} & 0 & 0 & 0 \\ 0 & 0 & 0 & \frac{1}{3} & \frac{1}{3} & \frac{1}{3} \end{bmatrix} \quad (10)$$

Hence, the voltage equations have below form [25]:

$$\overrightarrow{\boldsymbol{u}_{s1,2}} = \begin{bmatrix} u_{s\alpha1} \\ u_{s\beta1} \\ u_{s\alpha2} \\ u_{s\beta2} \end{bmatrix} = \boldsymbol{R}_{\boldsymbol{\alpha\beta}} \begin{bmatrix} i_{s\alpha1} \\ i_{s\beta1} \\ i_{s\alpha2} \\ i_{s\beta2} \end{bmatrix} + \boldsymbol{L}_{\boldsymbol{\alpha\beta}} \frac{d}{dt} \begin{bmatrix} i_{s\alpha1} \\ i_{s\beta1} \\ i_{s\alpha2} \\ i_{\beta s2} \end{bmatrix} + \begin{bmatrix} e_{\alpha1} \\ e_{\beta1} \\ e_{\alpha2} \\ e_{\beta2} \end{bmatrix} \quad (11)$$

where $L_{\alpha\beta}$ is Inductance matrix in Stationary reference frame that is defined as [35]:

$$\boldsymbol{L}_{\boldsymbol{\alpha\beta}} = \begin{bmatrix} L_{ls} + L_m & 0 & L_m & 0 \\ 0 & L_{ls} + L_m & 0 & L_m \\ L_m & 0 & L_{ls} + L_m & 0 \\ 0 & L_m & 0 & L_{ls} + L_m \end{bmatrix} \quad (12)$$

where $R_{\alpha\beta}$ is a four by four diagonal matrix with identical stator resistance R_s. Electromagnetic torque after transformation is expressed by:

$$T_e = \frac{2}{3}(i_{s\alpha1}e_{\alpha1} + i_{s\beta1}e_{\beta1} + i_{s\alpha2}e_{\alpha2} + i_{s\beta2}e_{\beta2})/\omega_m \quad (13)$$

where ω_m is rotor mechanical speed.

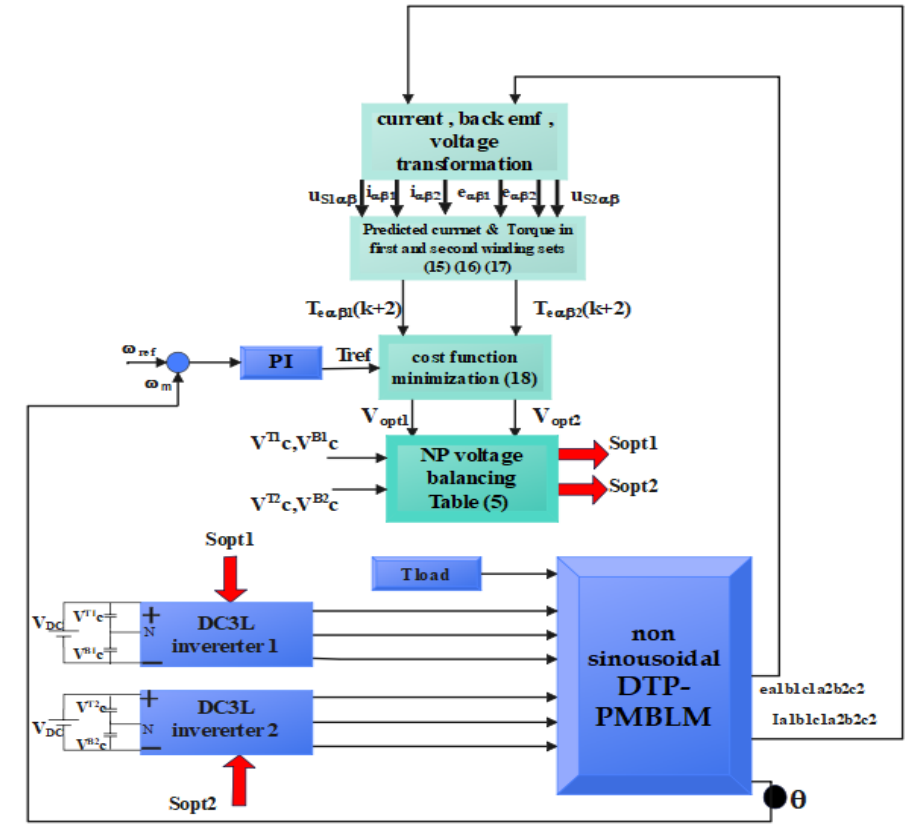

(a)

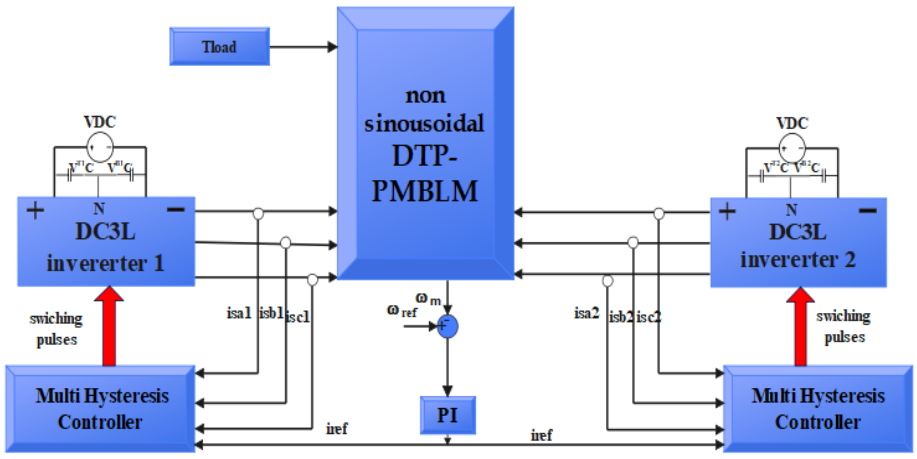

(b)

Fig. 3: (a) the suggested MPC scheme (b) the MHC controller scheme.

A. Neutral point voltage balancing

Unbalanced DC-link capacitor voltages cause current distortion, damage capacitors and increase torque ripple. Therefore, NP voltage should be around zero volts. For example, the small positive vector OPO increases the midpoint voltage and the small negative vector NON decreases the midpoint voltage [39], [40]. In this paper, small opposite vectors are chosen from the voltage vector diagram according to Table 3 that balance DC link capacitor voltages without weighting coefficients for the cost function. Hence, the control complication reduces due to lack of need to adjustment weighting coefficient. Therefore, the cost function in the suggested MPC method doesn't apply the NP voltage objective function similar to some references that have used the weighting coefficients [41].

Table 3: Optimal small vector for capacitor voltage balancing of first and second Inverter

	$V_{opt1}(V_3)$	$V_{opt1}(V_5)$	$V_{opt1}(V_7)$	$V_{opt1}(V_9)$	$V_{opt1}(V_{11})$	$V_{opt1}(V_{13})$
$V_c^{T1} \geq V_c^{B1}$	POO	PPO	OPO	OPP	OOP	POP
$V_c^{T1} < V_c^{B1}$	ONN	OON	NON	NOO	NNO	ONO
	$V_{opt2}(V_3)$	$V_{opt2}(V_5)$	$V_{opt2}(V_7)$	$V_{opt2}(V_9)$	$V_{opt2}(V_{11})$	$V_{opt2}(V_{13})$
$V_c^{T2} \geq V_c^{B2}$	POO	PPO	OPO	OPP	OOP	POP
$V_c^{T2} < V_c^{B2}$	ONN	OON	NON	NOO	NNO	ONO

B. Formulation of the cost function

For the suggested MPC strategy implementation, the Euler approximation could be used as:

$$\frac{dx}{dt} = \frac{x(k+1) - x(k)}{T_s} \tag{14}$$

where x is the control variable and T_s is the sampling time. The MPC technique uses the discrete equations of the system and derives the discrete model. By applying this approximation to (13), the (15) can be achieved which indicates future values of current in next sampling interval that is predicted the subsequent status of the system by the calculation of the next sampling time and by minimizing the cost function is specified the optimal switching modes.

$$\begin{bmatrix} i_{s\alpha1}(k+1) \\ i_{s\beta1}(k+1) \\ i_{s\alpha2}(k+1) \\ i_{s\beta2}(k+1) \end{bmatrix} = \frac{T_s}{\boldsymbol{L}} \left(\begin{bmatrix} u_{s\alpha1}(k) \\ u_{s\beta1}(k) \\ u_{s\alpha2}(k) \\ u_{s\beta2}(k) \end{bmatrix} - \begin{bmatrix} e_{\alpha1}(k) \\ e_{\beta1}(k) \\ e_{\alpha2}(k) \\ e_{\beta2}(k) \end{bmatrix} - \boldsymbol{R_{\alpha\beta}} * \begin{bmatrix} i_{s\alpha1}(k) \\ i_{s\beta1}(k) \\ i_{s\alpha2}(k) \\ i_{s\beta2}(k) \end{bmatrix} \right) + \begin{bmatrix} i_{s\alpha1}(k) \\ i_{s\alpha2}(k) \\ i_{s\beta1}(k) \\ i_{s\beta2}(k) \end{bmatrix} \tag{15}$$

It should be noted that half of the torque is produced by the first stator windings set and other half of the torque is produced by the second stator windings set. The predicted torque of the first and second stator windings set is described separately based on predicted current is expressed with the following equations:

$$T_{e1}(k+1) = \frac{3}{2}(i_{s1\alpha}(k+1) * e_{1\alpha}(k) + i_{s1\beta}(k+1)e_{1\beta}(k))/\omega_m \tag{16}$$

$$T_{e2}(k+1) = \frac{3}{2}(i_{s2\alpha}(k+1) * e_{2\alpha}(k) + i_{s2\beta}(k+1)e_{2\beta}(k))/\omega_m \tag{17}$$

The reference torque is produced by a PI controller. The aim of the suggested MPC strategy is to follow $T_{e\alpha\beta}(k+1)$ the reference torque. The suggested MPC scheme obtains the predicted torque utilizing (13)-(17).

The predicted and reference torque values of first and second stator windings set are compared in a cost function. All of 361 switching states are investigated and the state that minimizes the cost function as the next switching mode is exerted to the two DC3L inverters. To lessen the computational burden, the delay compensation technique is used. This strategy computes the predicted values in the shifted forward next sample value [42]. Consequently, cost function of the suggested MPC strategy is expresses as:

$$g = (0.5T_{eref} - T_{e\alpha\beta1}(k+2))^2 + (0.5T_{eref} - T_{e\alpha\beta2}(k+2))^2 \tag{18}$$

Fig. 4 represents the main part of the suggested MPC algorithm with minimizing the cost function. All 361 switching states will be searched.

```
k = 0;
g = zeros (361,1);
gop = inf;
opt = [1 1 1];
for i = 1:19
   V1 = V(:,:,i );
   for j = 1:19
      k = k+1;
      V2 = V(:,:,j);
      Vs1 = [real(T*V1'); imag(T*V1')];
      Vs2 = [real(T*V2'*exp(1i*pi/6));
imag(T*V2'*exp(1i*pi/6))];
      Vs = [Vs1;Vs2];
      isn1 = Ts*inv _L *(Vs-es-R*is) +is;
      Tn1 = (2/(3*C^2)) *([isn1(1) isn1(2)] *[es (1); es
(2)])/w;
      Tn2 = (2/(3*C^2)) *([isn1(3) isn1(4)] *[es (3); es
(4)])/w;
      g(k,1) = (0.5*Tref-Tn1) ^2+(0.5*Tref-Tn2) ^2;
      if g(k,1) <gop
         gop = g(k,1);
         opt = [i j];
      end
   end
end
```

Fig. 4: Main part of the suggested MPC algorithm.

Fig. 5 shows the flowchart for the MPC of non-sinusoidal DTP-PMBLM.

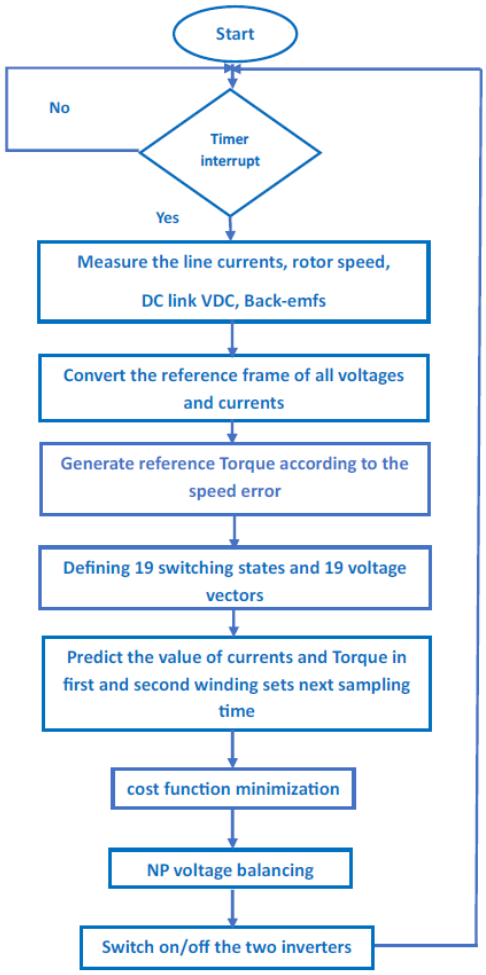

Fig. 5: The flowchart of the suggested MPC strategy for the Non-Sinusoidal DTP-PMBLM drive.

Results and Analysis

To simulate, MATLAB/Simulink is utilized to evaluate the suggested MPC strategy of in two DC3L inverters fed non-sinusoidal DTP-PMBLM. The DTP-PMBLM model is considered according to section of system configuration and modeling in the simulation. The system specifications are shown in Table 4.

To investigate the waveforms in the time interval of 0 to 0.4 s, reference speed of 350 rpm is applied to the non-sinusoidal DTP-PMBLM drive and the rotor direction is reversed from 350 rpm to -350 rpm in t=0.25 s with using speed command. At the start, the non-sinusoidal DTP-PMBLM drive works in no load mode and a constant load torque 73000 (N.m) is exerted to the system at t=0.1 s. Fig. 6 and Fig. 7 show the speed waveform, electromagnetic torque waveform of two set winding first and second, total electromagnetic torque waveform, current ia1 and ia2 and back-EMF ea1 and ea2 of the suggested MPC strategy and the MHC controller, respectively. As can be seen, both two control schemes present acceptable tracking performance of reference speed and acceptable tracking of full load torque in motoring and reverse conditions. Fig. 8 and Fig. 9 show the electromagnetic torque and current ripple with zoom in the suggested MPC strategy and MHC controller in bidirectional mode. According to Fig. 8(a) and Fig. 9(a), the torque ripples of the MHC controller and the suggested MPC strategy in motoring mode are 3200 (N.m) and 10000 (N.m), respectively and the torque ripples of the MHC controller and the suggested MPC strategy in reverse mode are 3200 (N.m) and 18000 (N.m), respectively. Thus, the suggested MPC strategy reduces the electromagnetic torque ripple 32% in motoring mode and 55.5% in reverse mode. Also, electromagnetic torque in the suggested MPC strategy scheme in comparison to the MHC controller scheme is smoother due to lack of current overshoots in commutation times. Moreover, Fig. 8(b) and Fig. 9(b) represent that the suggested MPC strategy has lower current ripple in comparison to the MHC controller. The current ripples of the MHC controller and the suggested MPC controller in motoring mode is 1000 A and 500 A, respectively and the current ripples of the MHC controller and the suggested MPC strategy in reverse mode are 1500 A and 700 A, respectively. Thus, the suggested MPC strategy reduces the current ripple 50% in motoring mode and 46.6% in reverse mode. Another advantage that suggested MPC strategy has over the MHC controller is that to decrease the torque response time. As shown in Fig. 6a and Fig. 6b, in moment of changing the direction of the motor, torque response time in the MHC controller is 0.06 s and the suggested MPC strategy is 0.01 s.

Table 4: Parameters of non-sinusoidal DTP-PMBLM

Parameter	Value
DC-link voltage V_{DC} (V)	4125
Rated Speed (rpm)	350
Power rating P (MW)	2.7
Rated torque (N.m)	73000
Pole Pairs (p)	20
Phase Resistance R (mΩ)	5.6
Phase Inductance (mH)	265
Mutual Inductance (mH)	110
Inertia constant (Kg.m^2)	60
Back-EMF constant (V/rpm)	0.923
Sampling interval (μs)	50
Capacitors C1 & C2 (F)	10

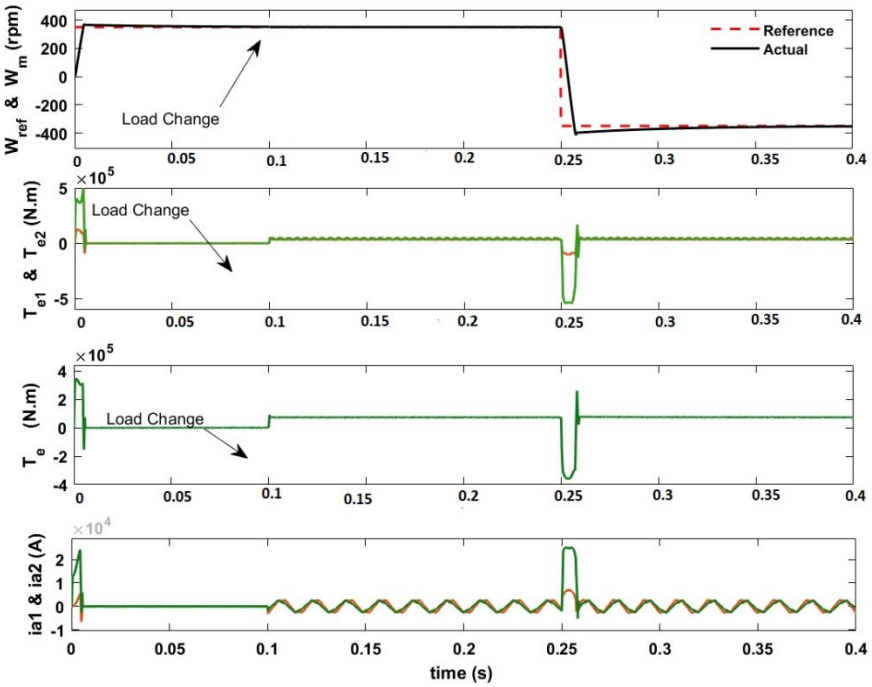

Fig. 6: Speed, electromagnetic torque of first and second winding sets, total electromagnetic torque, a1 and a2 phases current and back-EMFs of ea1 and ea2 waveforms of the suggested MPC strategy.

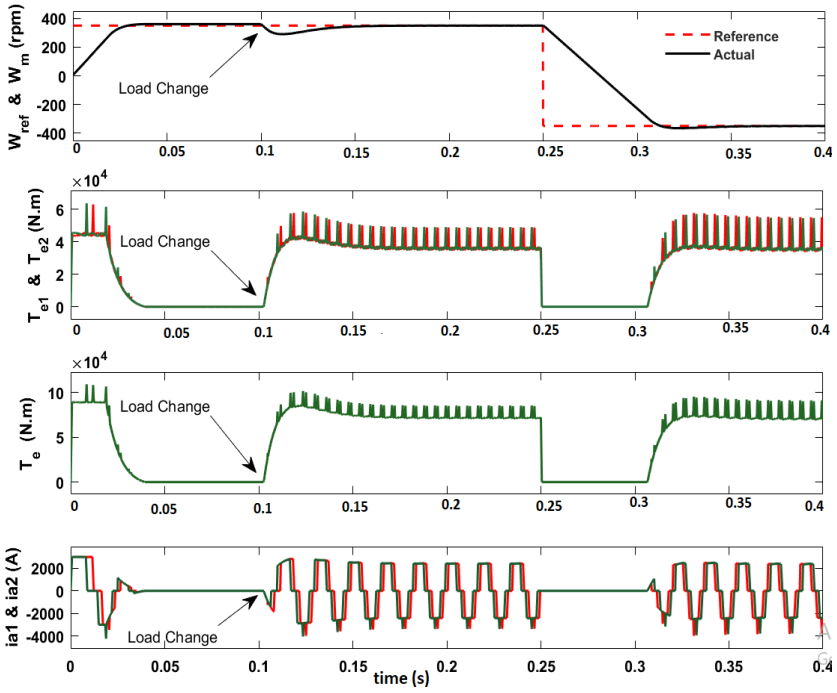

(a)

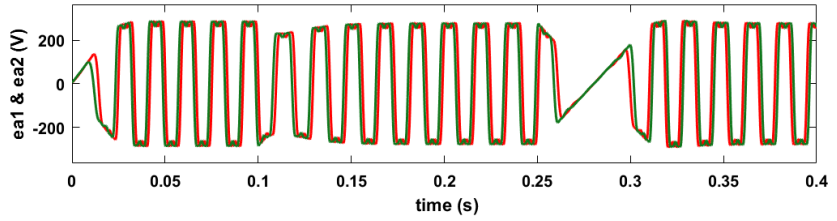

(b)

Fig. 7: Speed, electromagnetic torque of first and second winding sets, total electromagnetic torque, a1 and a2 phases current and back-EMFs of ea1 and ea2 waveforms of the MHC Controller.

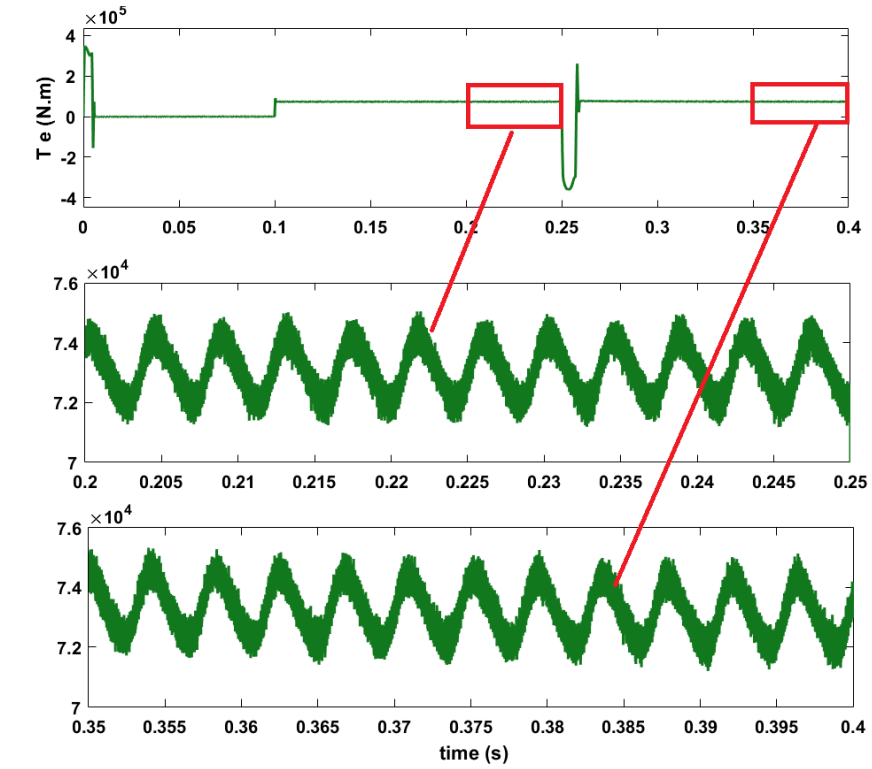

(a)

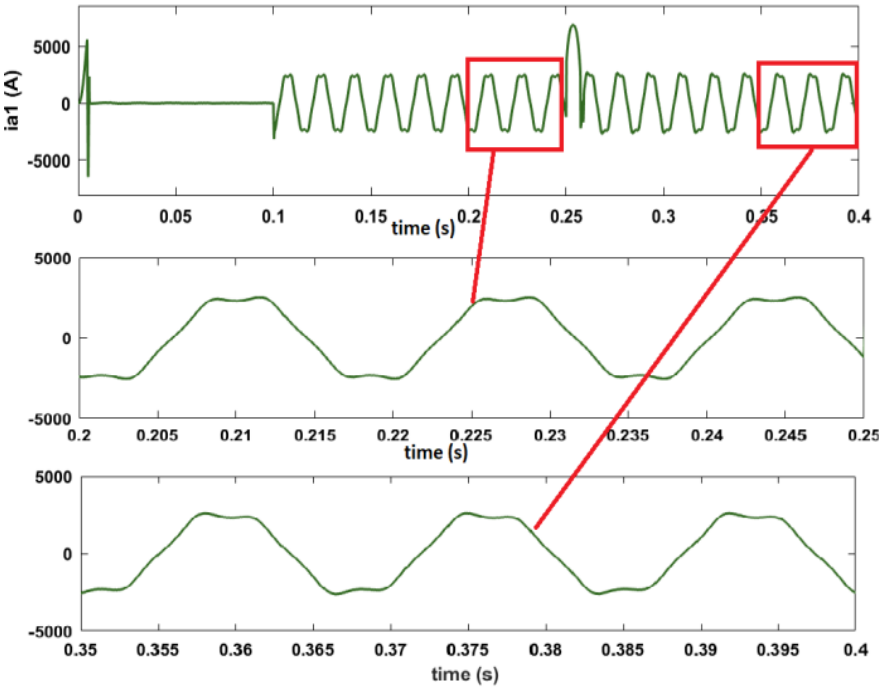

(b)

Fig. 8: a) Electromagnetic force ripple of with MPC method, b) a1 Phase current ripple of with MPC method.

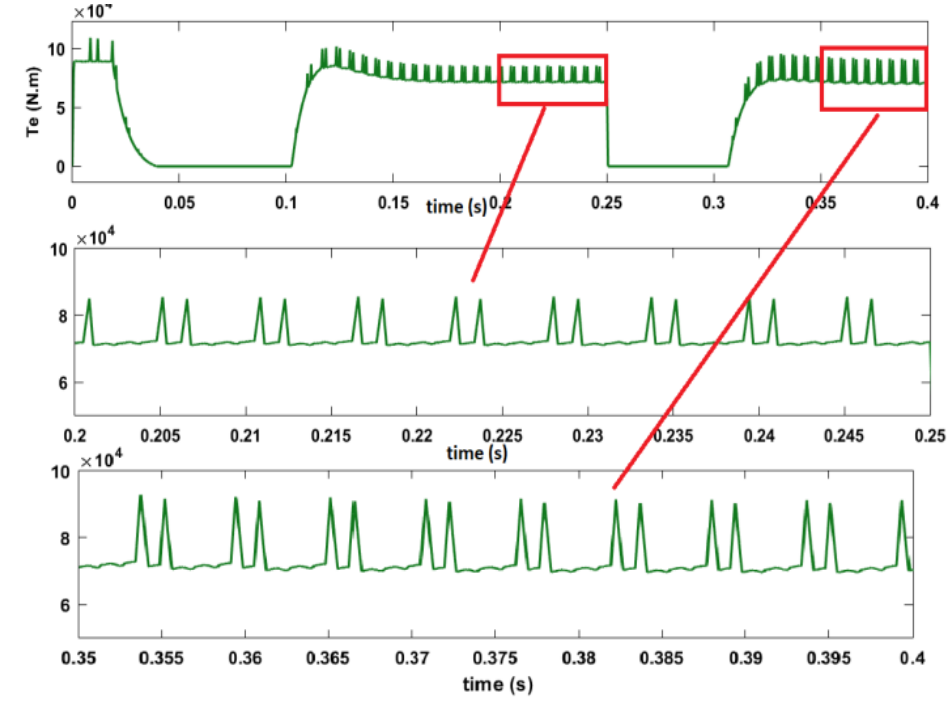

(a)

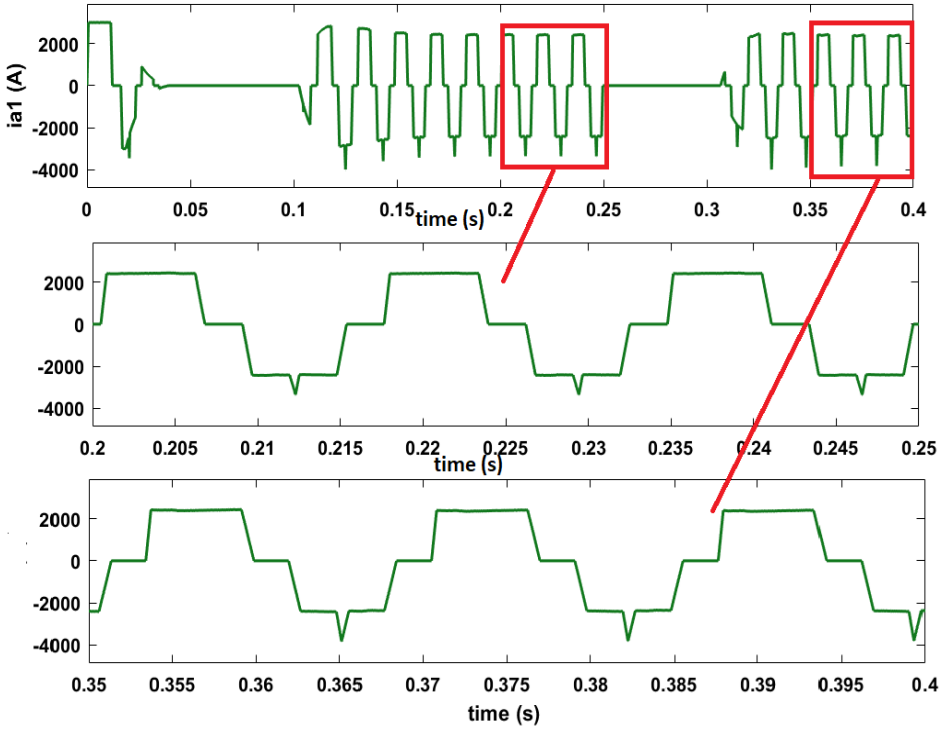

(b)

Fig. 9: a) Electromagnetic force ripple of with MHC method, b) a1 Phase current ripple of with MHC method.

Fig. 10 shows the electromagnetic torque response in unbalancing mode of capacitors voltage that provides higher electromagnetic torque ripple than balancing mode of capacitors voltage. The torque ripples with and without balancing of capacitors voltage in motoring mode and reverse mode is 8000 and 10000 (N.m), respectively.

Fig. 11(a) and Fig. 11(b) show the DC link capacitor voltage waveforms in suggested MPC strategy with scheme applied of balancing the DC link capacitor voltages described in section of system configuration and modeling. As can be observed, difference between the up and low capacitors voltages in balancing mode has a small error.

Robusteness Analysis

FCS-MPC method should to robust against parameters changes. In order to investigate the robustness of suggested strategy the stator resistance and the stator inductance are changed by ±15% in the simulation. The value of speed error and torque ripple are expressed in Table 5.

According to these results, the control operation is not destroyed when the parameters change from their real value, therefore the control strategy robustness is confirmed.

Table 6 compares two control methods quantitatively and qualitatively.

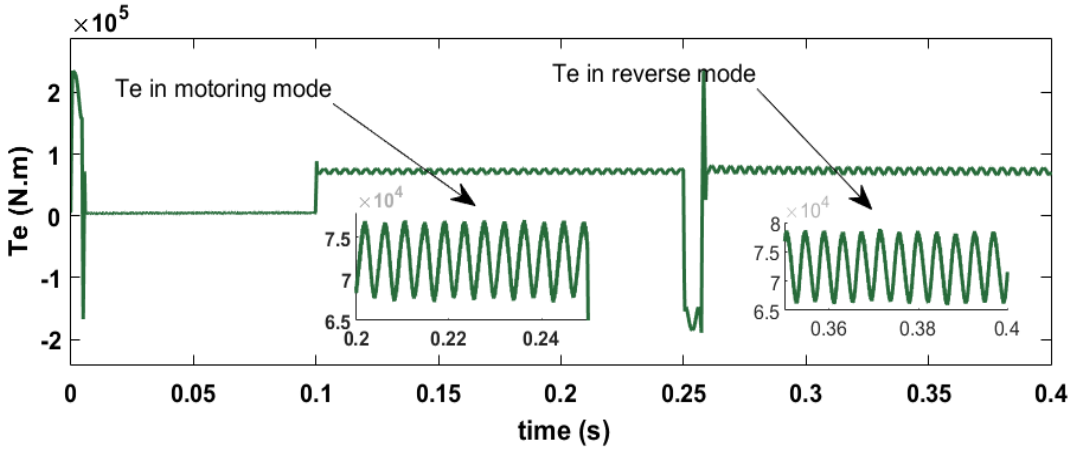

Fig. 10: The electromagnetic torque response in unbalancing mode.

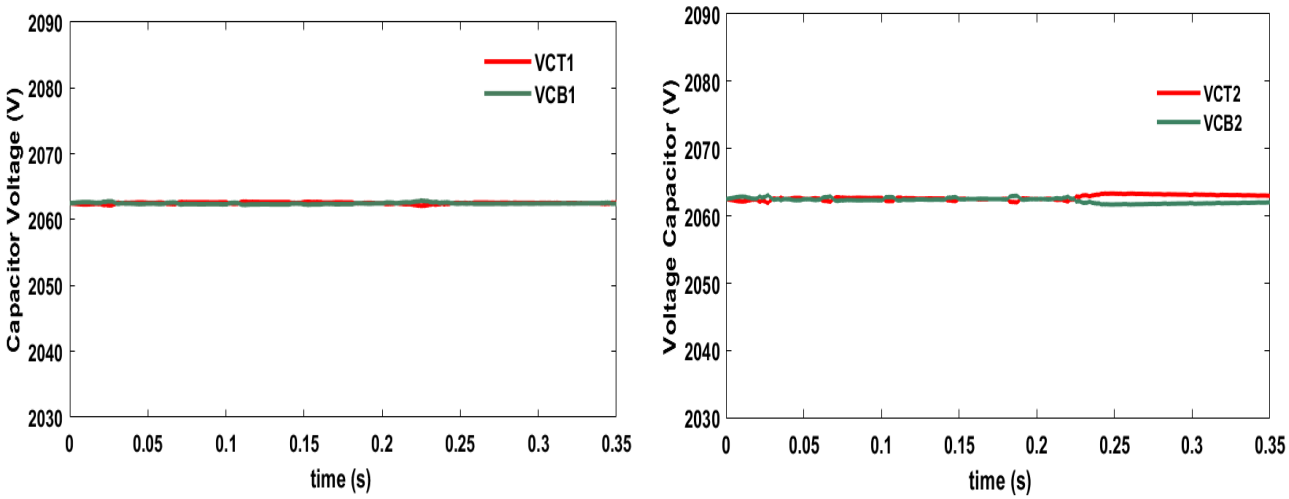

(a) (b)

Fig. 11: DC-link capacitor voltages waveforms in suggested MPC strategy with rated constant speed and torque in balancing modes a) balanced capacitor voltages of first DC3L inverter b) balanced capacitor voltages of second DC3L inverter.

Table 5: Robustness analysis

	L_m change		R_s change	
	Increase	Decrease	Increase	Decrease
	15%	15%	15%	15%
$\Delta\omega_m(\%)$	1.99	2.05	2.01	1.98
$\Delta T_e(\%)$	1.07	1.07	1.06	1.08

Table 6: Quantitative and qualitative comparison of two control strategy

Parameter		Methods	
		MHC	Suggested MPC
Speed tracking		Low	High
$\Delta T_e\left(N.m\right)$	$\omega_{ref}=350rpm$	10000	3200
$\Delta T_e\left(N.m\right)$	$\omega_{ref}=-350rpm$	18000	3200
$\Delta T_{e\max}/T_e$	$\omega_{ref}=350rpm$	13.7%	4.38%
$\Delta T_{e\max}/T_e$	$\omega_{ref}=-350rpm$	24.65%	4.38%
$\Delta T_e\left(N.m\right)$	$\omega_{ref}=350rpm$ without capacitor balancing		8000
$\Delta T_{e\max}/T_e$	$\omega_{ref}=350rpm$ without capacitor balancing		10.9%
Torque smoothness		Poor	High
$\Delta Is\left(A\right)$	$\omega_{ref}=350rpm$	1000	500
$\Delta Is\left(A\right)$	$\omega_{ref}=-350rpm$	1500	700
$\Delta Is_{\max}/Is$	$\omega_{ref}=350rpm$	36%	10%
$\Delta Is_{\max}/Is$	$\omega_{ref}=-350rpm$	60%	32%
Commutation oscillations		High	Low
Torque response time		0.06 s	0.01 s

Proposed Fault-Tolerant Schemes

The purpose of FTC is to allow operation to continue with minimal performance degradation. In this research, FTC schemes are presented for two prevalent electrical fault types, open switch fault Sa1 in the first leg of the first DC3L inverter and open phase fault. In the FTC scheme, the mathematical model of the motor and the control strategy do not change, and therefore, the proposed FTC scheme is not complex.

A. Open Switch Fault (Sa1)

When the open switch fault occurs in switch Sa1, the DC3L inverter does not generate a P level in leg a1 the first inverter. Therefore, the open switch fault of Sa1 causes the inverter switching states with P level in leg a1 to be eliminated. Remaining switching states of the first DC3L inverter for open switch fault Sa1 has been shown in Fig. 12.

It is considered that the open switch fault occurs at t=0.2, as shown in Fig. 13, with the occurrence of the fault, the torque and speed will face with a strong ripple and fluctuation. To control the fault tolerance, the cost function is changed to the following equation:

$$g=(T_{eref}-T_{e\alpha\beta1}(k+2))^2+(T_{eref}-T_{e\alpha\beta2}(k+2))^2 \quad (19)$$

Fig. 14 shows that the speed and torque waveforms oscillate at the moment t = 0.2 s, and after a few oscillations, both waveforms stabilize and the torque and speed ripples decrease.

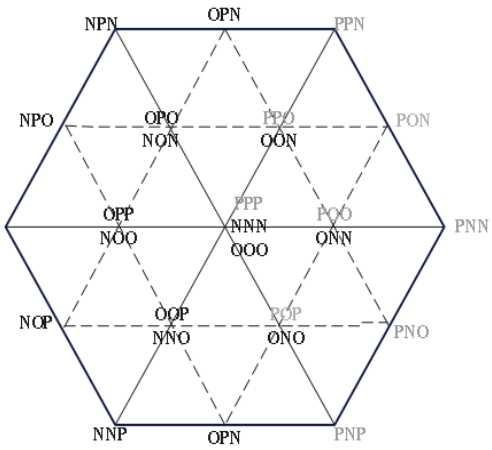

Fig. 12: Remaining switching states of the first DC3L inverter for open switch fault Sa1.

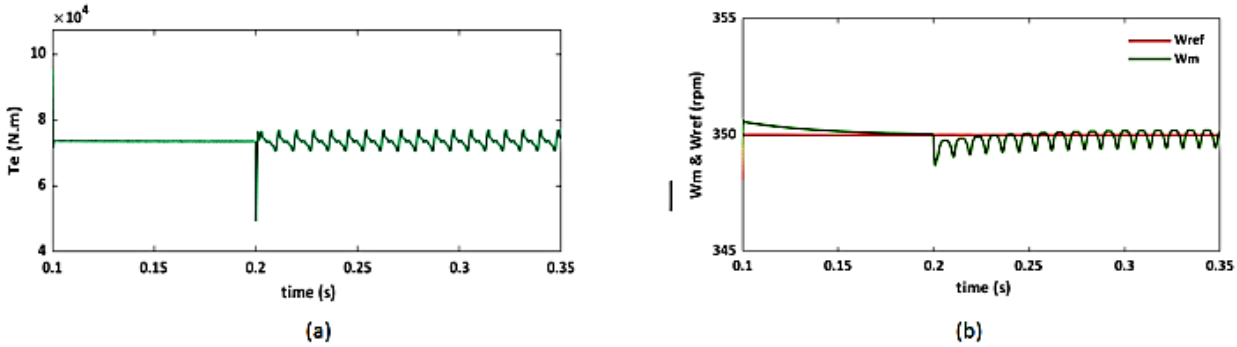

Fig. 13: Fault occurrence for open switch fault Sa1 at t=0.2s a) Torque waveform b) Speed waveform.

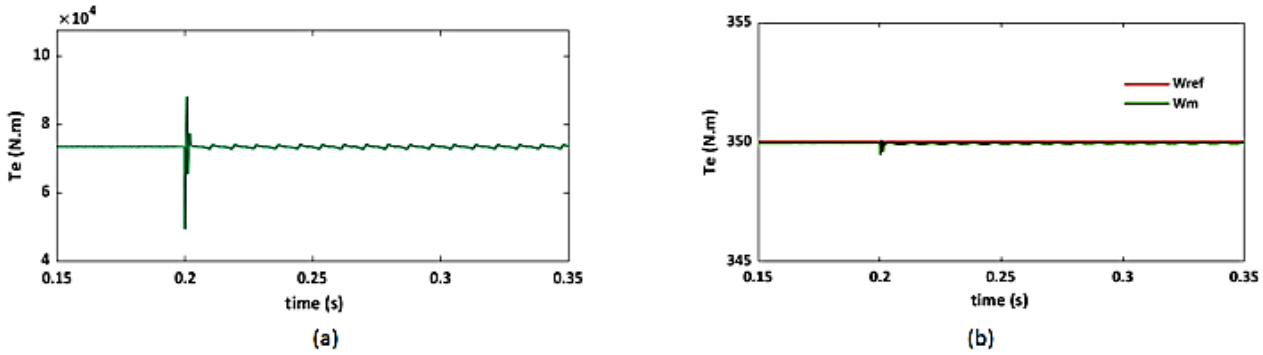

Fig. 14: FTC scheme for open switch fault Sa1 at t=0.2s a) Speed waveform b) Torque waveform.

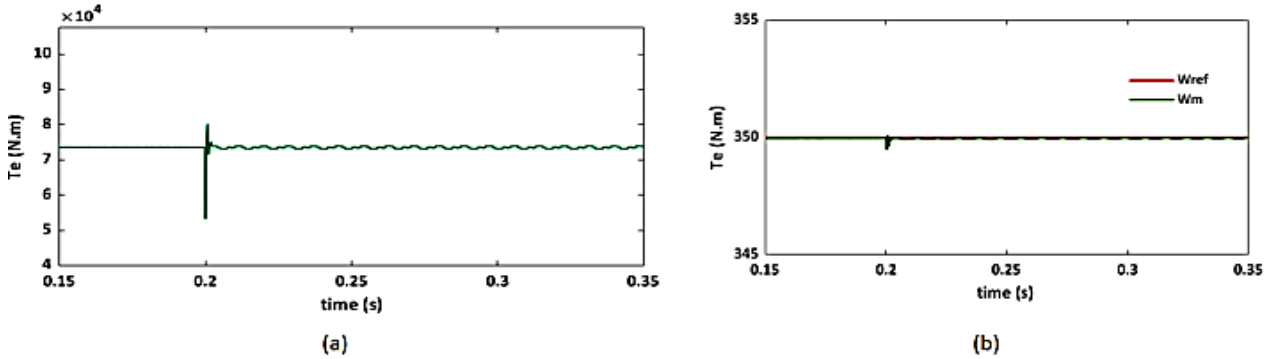

Fig. 15: Fault occurrence for open phase fault in a1 phase at t=0.2s a) Torque waveform b) Speed waveform.

B. Open Phase Fault in a1 Phase

In this paper, instead of creating a new mathematical model for the faulty motor with open phase fault in a1 phase, the faulty motor is directly assumed healthy. In this method, no changing in the mathematical modelling, space vector diagram of two inverters and control format of the motor drive is required, and the total complication of the FTC is reduced.

As can be observed in Fig. 15, the speed and torque ripple have increased at the instant t = 0.2s. The six-phase current waveforms with fixed speed and torque of 350 rpm and 73000 (N.m) in the open phase fault of phase a1 at the instant t = 0.2s are shown in Fig. 16. As can be observed, the six-phase winding currents under no-fault conditions have the same amplitude and the maximum phase current is 2500 A. After t = 0.2s, the a1 phase winding is cut off from the inverter and the a1 phase current becomes zero.

As can be seen, after t = 0.2s, the other five phase winding currents have different amplitudes than the healthy state.

By modifying the cost function according to (20), FTC scheme for an open phase is obtained. This cost function distributes the current in the ratio of 0.4 and 0.6 between the first set winding and the second set winding, which reduces the current amplitude of the windings and subsequently reduces the torque ripple.

$$g = (0.4T_{eref} - T_{e\alpha\beta1}(k+2))^2 + (0.6T_{eref} - T_{e\alpha\beta2}(k+2))^2 \quad (20)$$

As shown in Fig. 17, the speed and torque waveforms have less ripple. Also, Fig. 18 shows phases current waveforms with constant speed and torque of 350 rpm and 73000 (N.m) at open phase fault a1 at t=0.2s by applying the FTC scheme. Table 7 shows the calculated results in healthy, faulty and postfault modes, including peak current, average torque, torque ripple, speed, and speed change.

In addition, the results of harmonic analysis of phases b1, c1, a2, b2, c2 current are represented in Fig. 19. According to this figure, when the motor changes from the healthy operation mode to the faulty mode, the fundamental amplitude and the third, fifth, and seventh harmonics of the phases current of b1, c1, a2, b2, c2 increase and by applying the FTC strategy, the amplitude of the current and the first, third, fifth, and seventh harmonics decrease.

It should be mentioned, in Multiphase motors with odd phase numbers, zero-sequence components do not exist in any star-connected with an isolated neutral point, hence the zero-sequence currents cannot flow [43].

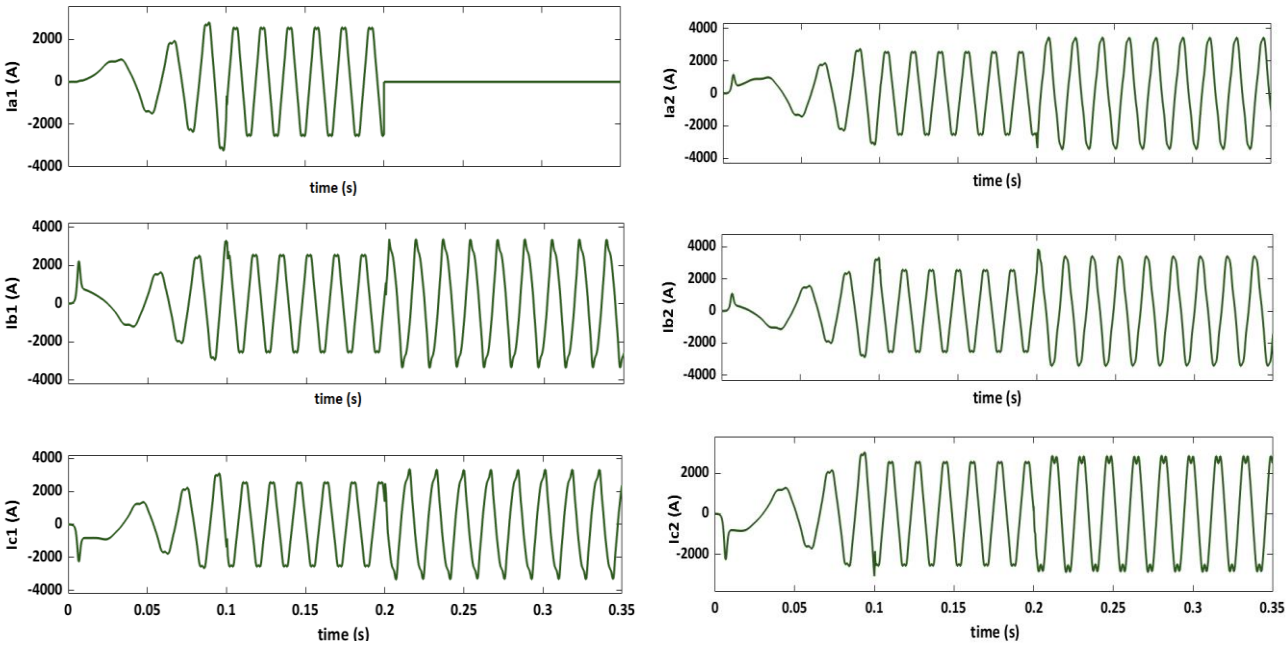

Fig. 16: Phases current waveform with constant speed and torque of 350 rpm and 73000 (N.m) in open phase fault of at t=0.2s.

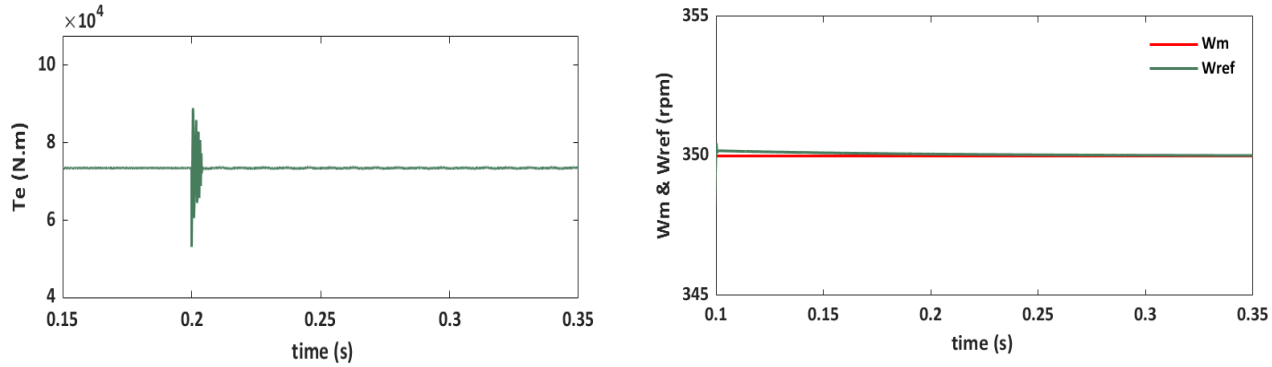

(a) (b)

Fig. 17: FTC scheme for open phase fault of a1 phase at t=0.2s a) Torque waveform b) Speed waveform.

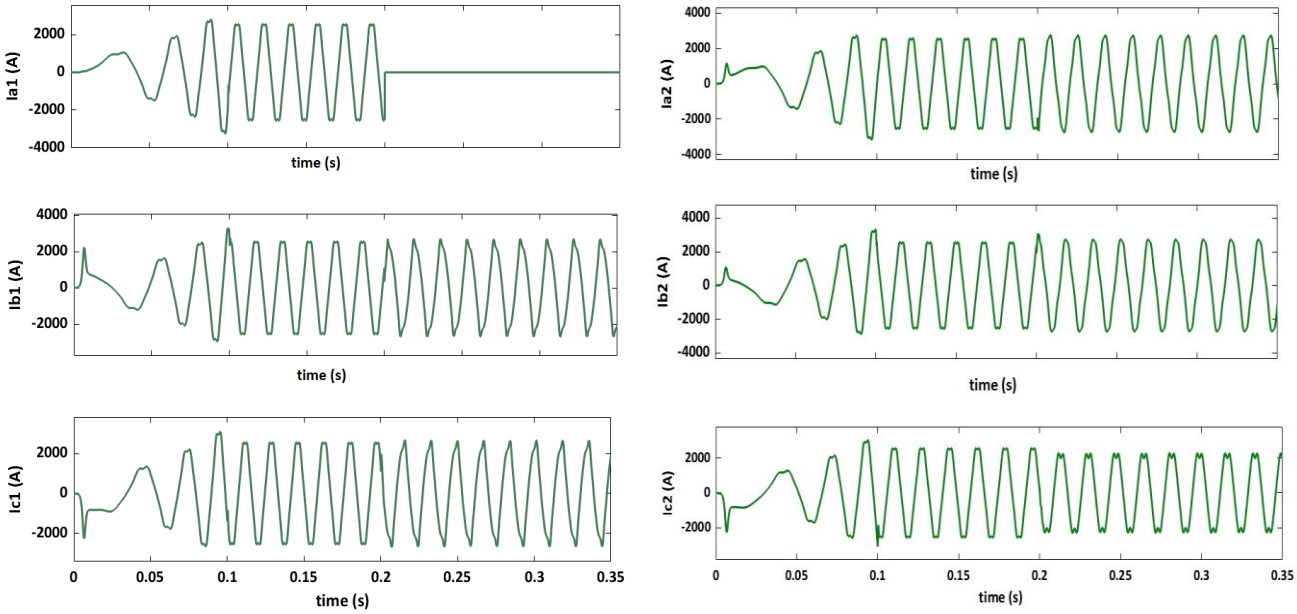

Fig. 18: phases current waveforms with constant speed and torque of 350 rpm and 73000 (N.m) at open phase fault a1 at t=0.2s by applying the FTC scheme.

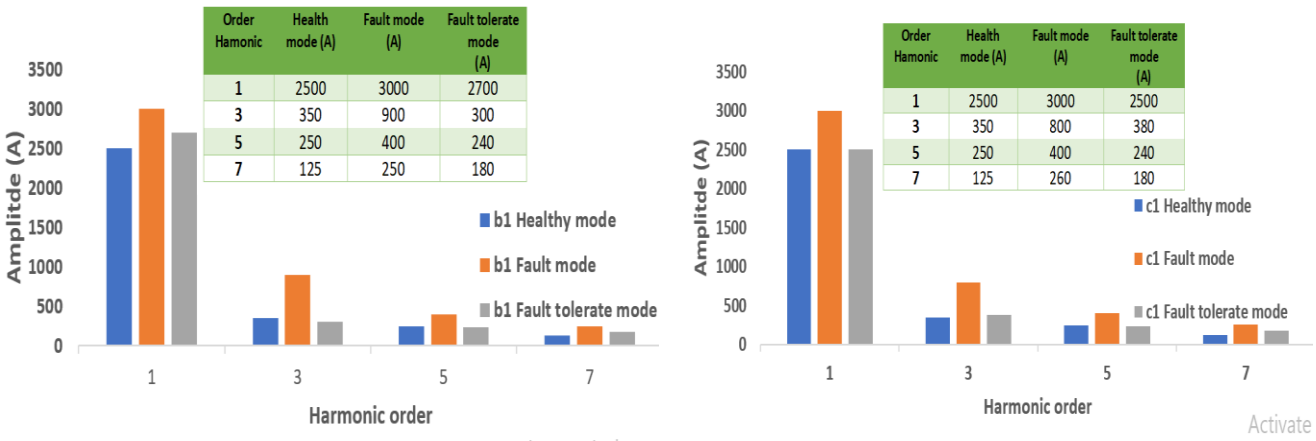

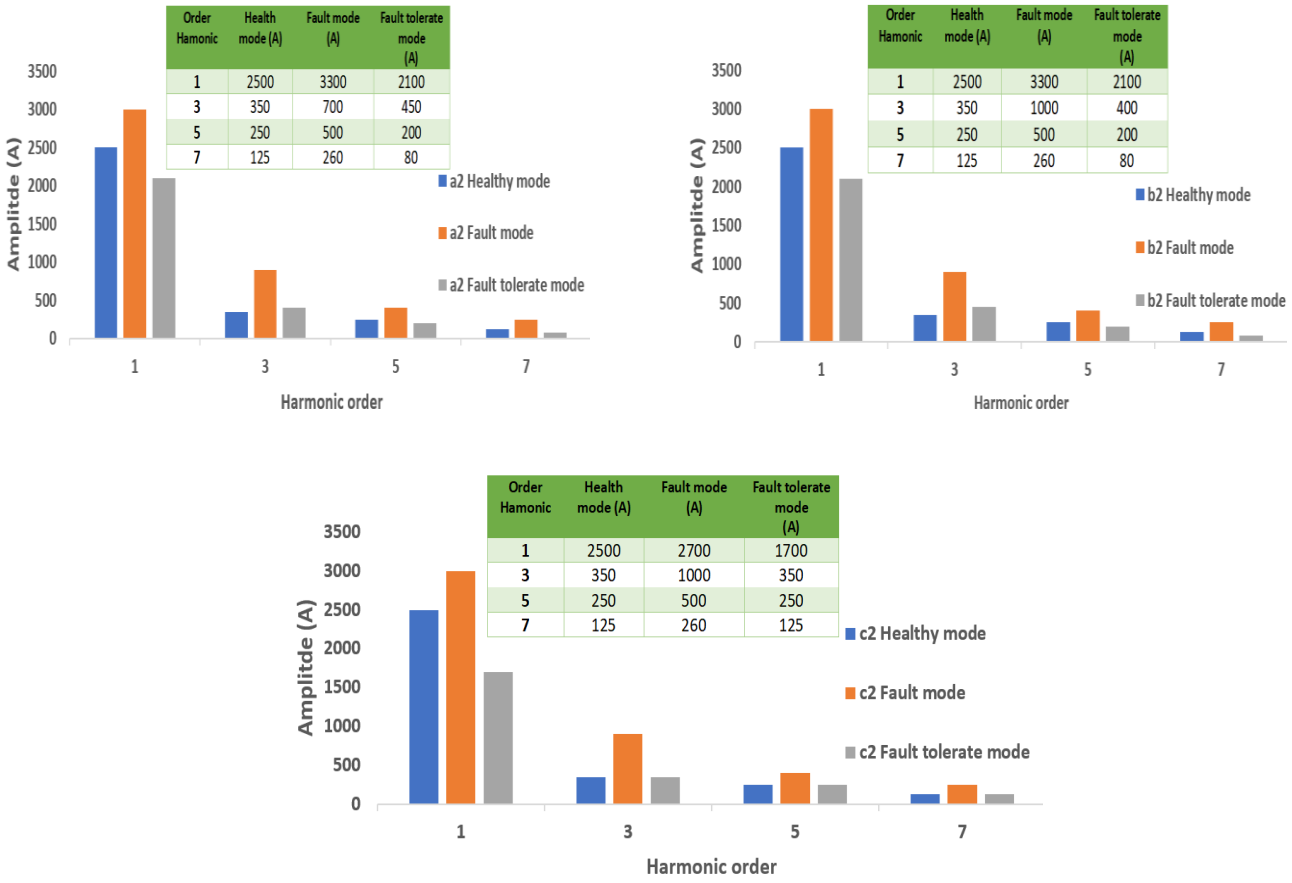

Fig. 19: Results of harmonic analysis of current of phases b1, c1, a2, b2, c2.

Table 7: Calculated results in healthy, faulty and postfault modes, including peak current, average torque, torque ripple, speed, and speed change

	Peak current (A)						T_{eave} $(N.m)$	$\Delta T_e(\%)$	ω_m (rpm)	Δω(%)
Open Phase a1	a1	b1	c1	a2	b2	c2				
Healthy mode	2500	2500	2500	2500	2500	2500	73500	4.38	350	0
Fault mode	0	3000	3000	3300	3400	2700	73500	8.5	350	0.2
fault tolerate control mode	0	2700	2500	2100	2100	1700	73500	5.8	350	0.05

Conclusions

This paper suggested a optimization MPC strategy to reduce torque ripple of the DTP-PMBL drive fed by two DC3L inverters for the application of medium voltage rating which are sensitive to noise and ripple. The torque and current ripple of the suggested MPC strategy are improved compared to the MHC control. In addition, the suggested MPC strategy tracks the actual speed and the reference speed of the rotor with high accuracy. The voltage balancing of the capacitors in both the DC3L inverters was simply done without the need for a weighting coefficient. The electromagnetic torque ripple in balancing mode of capacitors voltage is lower than unbalancing mode of capacitors voltage in the suggested MPC controller. The simulation results prove the advantages of the suggested MPC strategy against the MHC controller, which are expressed as follows:

- Faster dynamic torque response time up to 16.67% of the suggested MPC strategy than the MHC controller;
- Lower torque ripple the suggested MPC strategy than the MHC controller up to 32% in motoring

mode and 55.5% in reverse mode;

- Current ripple up to 50% the suggested MPC strategy than the MHC controller in motoring mode and 46.6% in reverse mode;
- Lower torque ripple the suggested MPC strategy than the suggested MPC strategy without unbalancing up to 40% in motoring mode and 35.5% in reverse mode;
- Reduction of torque ripple up to 68% and speed ripple up to 25% of fault tolerate control the suggested MPC strategy than faulty mode in open switch fault;
- Reduction of torque ripple up 33% to and speed ripple up to 80% of fault tolerate control the suggested MPC strategy than faulty mode in open switch fault;
- Reduction of the fundamental amplitude and the third, fifth, and seventh harmonics of the phases current of b1, c1, a2, b2, c2 by applying the FTC strategy.

Author Contributions

Z. Emami carried out the simulation results. A. Halvaie confirmed the results. Z. Emami and Edited the manuscript.

Acknowledgment

The authors thankfully appreciate the anonymous reviewers and the editor of JECEI for their useful comments and suggestions.

Funding

This research received no external funding.

Conflict of Interest

The authors declare no potential conflict of interest regarding the publication of this work. In addition, the ethical issues including plagiarism, informed consent, misconduct, data fabrication and, or falsification, double publication and, or submission, and redundancy have been completely witnessed by the authors.

Abbreviations

MHC	Multiband Hysteresis Current
BLDCM	Brushless DC Motors
PMBLM	Permanent Magnet Brushless Motors
FCS-MPC	Finite Control Set Model Predictive Control
DC3L	Diode-clamped three-level
DTP-PMSM	Dual Three Phase Permanent Magnet Synchronous Motors
FOC	Field Oriented Control
MV	Medium Voltage
DTC	Direct Torque Control
NP	Neutral Point
FTC	Fault Tolerate Control

References

[1] E. Levi, "Multiphase electric machines for variable-speed applications," IEEE Trans. Ind. Electron., 55(5): 1893-1909, 2008.

[2] F. Barrero, M. J. Duran, "Recent advances in the design, modeling, and control of multiphase machines—part I," IEEE Trans. Ind. Electron., 63(1): 449-458, 2016.

[3] M. Mengoni, L. Zarri, A. Tani, L. Parsa, G. Serra, D. Casadei, "High-Torque-density control of multiphase induction motor drives operating over a wide speed range," IEEE Trans. Ind. Electron., 62(2): 814-825, 2015.

[4] Z. Zhu, S. Wang, B. Shao, L. Yan, P. Xu, Y. Ren, "Advances in dual-three-phase permanent magnet," Energies, 14(22): 7508, 2021.

[5] A. Dey, P. P. Rajeevan, R. Ramchand, K. Mathew, K. Gopakumar, "A space-vector-based hysteresis current controller for a general n-level inverter-fed drive with nearly constant switching frequency control,"IEEE Trans. Ind. Electron., 60(5): 1989-1998, 2013.

[6] L. BK, M. Ehsani, "Advanced simulation model for brushless DC motor drives," Electr. Power Components Syst., 31(9): 841-868, 2003.

[7] O. Fall, N. K. Nguyen, J. F. Charpentier, P. Letellier, E. Semail, X. Kestelyn, "Variable speed control of a 5-phase permanent magnet synchronous generator including voltage and current limits in healthy and open-circuited modes," Electr. Power Syst. Res., 140: 507-516, 2016.

[8] A. Taheri, A. Rahmati, S. Kaboli, "Efficiency improvement in DTC of six-phase induction machine by adaptive gradient descent of flux," IEEE Trans. Power Electron., 27(3): 1552-1562, 2012.

[9] H. Afsharirad, S. Misaghi, "Torque ripple reduction by using virtual vectors in direct torque control method using neutral-point-clamped inverter," J. Electr. Comput. Eng. Innovations, 13(1): 197-208, 2025.

[10] X. Kestelyn, E. Semail, "A vectorial approach for generation of optimal current references for multiphase permanent-magnet synchronous machines in real time," IEEE Trans. Ind. Electron., 58(11): 5057-5065, 2011.

[11] M. Bermudez, O. Gomozov, X. Kestelyn, F. Barrero, N. K. Nguyen, E. Semail, " Model predictive optimal control considering current and voltage limitations: real-time validation using OPAL-RT technologies and five-phase permanent magnet synchronous machines," Math. Comput. Simul., 158: 148-161, 2019.

[12] C. Martín, M. Bermúdez, F. Barrero, M. R. Arahal, X. Kestelyn, M. J. Durán, "Sensitivity of predictive controllers to parameter variation in five-phase induction motor drives," Control Eng. Pract., 68: 23-31, 2017.

[13] M. Schweizer, T. Friedli, J.W. Kolar, "Comparative evaluation of advanced three-phase three-level inverter/converter topologies against two-level systems," IEEE Trans. Ind. Electron., 60(12): 5515–5527, 2013.

[14] M. Habibullah, D. D. C. Lu, D. Xiao, M. F. Rahman, "Finite-state predictive torque control of induction motor supplied from a three-level NPC voltage source inverter," IEEE Trans. Power Electron., 32(1): 479-489, 2016.

[15] Y. Hu, Z.Q. Zhu, M. Odavic, "Comparison of two-individual current control and vector space decomposition control for dual three-phase PMSM," IEEE Trans. Ind. Appl., 53(5): 4483-4492. 2017.

[16] K. H. Kim, M. J. Youn, "DSP-based high-speed sensorless control for a brushless DC motor using a DC link voltage control," Electr. Power Compon. Syst., 30(9): 889-906, 2002.

[17] G. Scarcella, G. Scelba, M. Pulvirenti, R. D. Lorenz, "Fault-tolerant capability of deadbeat-direct torque and flux control for three-phase pmsm drives," IEEE Trans. Ind. Appl., 53(6): 5496-5508, 2017.

[18] H. Berriri, W. Naouar, I. Bahri, I. Slama-Belkhodja, E. Monmasson, "Field programmable gate array-based fault-tolerant hysteresis current control for Ac machine drives," IET Elect. Power Appl., 6(3): 181-189, 2012.

[19] F. Aghili, "Fault-tolerant torque control of BLDC motors," IEEE Trans. Power Electron., 26(2): 355-363, 2011.

[20] G. Scarcella, G. Scelba, M. Pulvirenti, R. D. Lorenz, "Fault-tolerant capability of deadbeat-direct torque and flux control for three-phase PMSM drives," IEEE Trans. Ind. Appl., 53(6): 5496-5508, 2017.

[21] Z. Liu, Y. Li, Z. Zheng, "A review of drive techniques for multiphase machines," CES Trans. Electr. Mach. Syst., 2(2): 243-251, 2018.

[22] M. B. Guzman, "Novel control techniques in multiphase drives: Direct control methods (DTC and MPC) under limit situations," PhD, École Nationale Supérieure d'Arts et Métiers, 2018.

[23] H. Zhou, G. Liu, W. Zhao, X. Yu, M. Gao, "Dynamic performance improvement of five-phase permanent-magnet motor with short-circuit fault," IEEE Trans. Ind. Electron., 65(1): 145-155, 2018.

[24] H. Zhou, W. Zhao, G. Liu, R. Cheng, Y. Xie, "Remedial field-oriented control of five-phase faulttolerant permanent-magnet motor by using reduced-order transformation matrices," IEEE Trans. Ind. Electron., 64(1): 169-178, 2017.

[25] H. Zhou, G. Liu, W. Zhao, X. Yu, M. Gao, "Dynamic performance improvement of five-phase permanent-magnet motor with short-circuit fault," IEEE Trans. Ind. Electron., 65(1): 145-155, 2018.

[26] B. Tian, Q. T. An, J. D. Duan, D. Y. Sun, L. Sun, D. Semenov, "Decoupled modeling and nonlinear speed control for five-phase pm motor under single-phase open fault," IEEE Trans. Power Electron., 32(7): 5473-5486, 2017.

[27] G. Liu, Z. Lin, W. Zhao, Q. Chen, G. Xu, "Third harmonic current injection in fault-tolerant five-phase permanent-magnet motor drive," IEEE Trans. Power Electron., 33(8): 6970-6979, 2018.

[28] C. Xiong, H. Xu, T. Guan, P. Zhou, "Fault-tolerant FOC for five-phase SPMSM with non-sinusoidal back EMF," IET Electr. Power Appl., 13(11): 1734-1742, 2019.

[29] M. Bermudez, I. Gonzalez-Prieto, F. Barrero, H. Guzman, X. Kestelyn, M. J. Duran, "An experimental assessment of open-phase fault-tolerant virtual-vector-based direct torque control in five-phase induction motor drives," IEEE Trans. Power Electron., 33(3): 2774-2784, 2018.

[30] A. Mohammadpour, L. Parsa, "Global fault-tolerant control technique for multiphase permanentmagnet machines," IEEE Trans. Ind. Appl., 51(1): 178-186, 2015.

[31] Z. Liu, Z. Zheng, Y. Li, "Enhancing fault-tolerant ability of a nine-phase induction motor drive system using fuzzy logic current controllers," IEEE Trans. Energy Convers., 32(2): 759-769, 2017.

[32] M. Gu, Z. Wang, K. Yu, X. Wang, Ming Cheng, "Interleaved model predictive control for three-level neutral-point-clamped dual three-phase PMSM drives with low switching frequencies, " IEEE Trans. Power Electron., 36(10): 11618-11630, 2021.

[33] A. Tani, G. Serra, M. Mengoni, L. Zarri, G. Rini, D. Casadei, "Dynamic stator current sharing in quadruple three-phase induction motor drives, " in Proc. the 39th Annual Conference of the IEEE Industrial Electronics Society (IECON): 5173-5178., 2013.

[34] S. Hu, Z. Liang, W. Zhang, X. He, "Research on the integration of hybrid energy storage system and dual three-phase PMSM drive in EV," IEEE Trans. Ind. Electron. 65(8): 6602-6611, 2018.

[35] P. Drozdowski, "Modelling of BLDCM with a double 3-phase stator winding and back EMF harmonics," Arch. Electr. Eng., 64(1): 53-66, 2015.

[36] B. Wu, M. Narimani, "High-power converters and AC drives," IEEE Press WILEY, 2017.

[37] R. A. Raj, M. P. Shreelakshmi, S. George, "Multiband hysteresis current controller for three level BLDC motor drive," in Proc. International Conference on Power, Instrumentation, Control and Computing (PICC), 2020.

[38] C. Bian, X. Li, G. Zhao, "The peak current control of permanent magnet brushless DC machine with asymmetric dual-three phases," CES Trans. Electr. Mach. Syst., 2(1): 129-135, 2018.

[39] N. Celanovic, D. Boroyevich, "A comprehensive study of neutral-point voltage balancing problem in three-level neutral-point-clamped voltage source PWM Inverters," IEEE Trans. Power Electron., 15(2): 242-249, 2000.

[40] C. Xue, D. Zhou, Y. Li, "Finite-control-set model predictive control for three-level NPC inverter-fed PMSM drives with LC filter, " IEEE Trans. Ind. Electron., 68(12): 11980-11991, 2021.

[41] J. Chen, Z. Wang, Y. Wang, M. Cheng, "Analysis and control of NPC-3L inverter fed dual three-phase PMSM Drives considering their asymmetric factors," J. Power Electron., 17(6): 1500-1511, 2017.

[42] Y. Lue, C. Liu, "A flux constrained predictive control for a six-phase PMSM motor with lower complexity," IEEE Trans. Ind. Electron., 66(7): 5081-5093, 2019.

[43] M. A. Frikha, J. Croonen, K. Deepak, Y. Benômar, M. El Baghdadi, O. Hegazy, "Multiphase motors and drive systems for electric vehicle powertrains: State of the art analysis and future trends," Energies, 16(2): 768, 2023.

Biographies

Zahra Emami was born in Isfahan, Iran, in 1981. She received M.Sc. degrees from Isfahan University of Technology, Iran. She is currently a Ph.D. student in University of Kashan, Kashan, Iran. Her research interests include power electronics, control of electrical motor drives. Ms. Emami was the recipient of the IEEE 1th Power Electronics, Drive Systems, and Technologies Conference (PEDSTC'10) best paper award in 2010.

- Email: zahra_emami1765@yahoo.com
- ORCID: 0009-0000-4054-2822
- Web of Science Researcher ID: NA
- Scopus Author ID: NA
- Homepage: NA

Abolfazl Halvaei Niasar (S'04–M'06–SM'14) was born in Kashan, Iran in 1974. He received his B.Sc., M.Sc., and Ph.D. in 1996, 1999, and 2008 from Isfahan University of Technology (IUT), University of Tehran (UT) and Iran University of Science and Technology (IUST) respectively, all in Electrical Engineering. He has joined the Department of Electrical and Computer Engineering at University of Kashan, Kashan, Iran since 2008 as assistant professor. He has authored more than 150 technical papers published in journals and conference proceedings. He is the

holder of two Iranian patents and has directed some industrial research projects. His current major research interests include PM and brushless DC motor (BLDC) drives, sensorless drives, design, analysis and control of electrical machines. Dr. Halvaei is senior member of the Institute of Electrical and Electronics Engineers, IEEE.

- Email: halvaei@kashanu.ac.ir
- ORCID: 0000-0003-4265-5120
- Web of Science Researcher ID: NA
- Scopus Author ID: 15846169600
- Homepage: https://faculty.kashanu.ac.ir/halvaei/fa